Cusped Electrical Conductivity in Spin-1 Chiral Fermion Systems Arising from Multifold Band Degeneracy

Risako Kikuchi ${^{\tiny{0}}}^{1*},\;\;$ Junya Endo ${^{\tiny{0}}}^{2\dagger}$ and Ai Yamakage ${^{\tiny{0}}}^{1\dagger}$

^{1*}Department of Physics, Nagoya University, Furo-cho, Chikusa-ku, Nagoya, 4648602, Aichi, Japan.

²Department of Physics, University of Tokyo, Hongo, Bunkyo, 1130033, Tokyo, Japan.

> *Corresponding author(s). E-mail(s): kikuchi.risako.i4@s.mail.nagoya-u.ac.jp; Contributing authors: endo@hosi.phys.s.u-tokyo.ac.jp; yamakage.ai.x6@f.mail.nagoya-u.ac.jp; †These authors contributed equally to this work.

Abstract

The energy-dependent electrical conductivity in spin-1 chiral fermion systems with disorder is studied using the self-consistent Born approximation. A distinct cusp-like feature appears at an energy different from the band-crossing point, arising from the multifold band-crossing structure formed by the Dirac and trivial bands. The energy position of the cusp and the corresponding value of the electrical conductivity are found to depend sensitively on both the impurity scattering strength and the curvature of the trivial band. These findings demonstrate the critical role of multifold band crossings and disorder-induced broadening of energy levels in determining the transport properties, offering theoretical insight into the unconventional conductivity behavior observed in topological semimetals hosting spin-1 chiral fermions.

Keywords: Topological Semimetal, Multifold Fermion, Electrical Conductivity, SCBA

1 Introduction

Topological semimetals are characterized by crossings of multiple energy bands, known as multifold fermions, and exhibit unique physical properties [1–3]. A minimal model for a multifold fermion is the spin-1/2 Dirac or Weyl fermion, which arises from the crossing of two linear bands. Another notable case is the threefold band degeneracy, consisting of two linear bands and one nearly flat (or "trivial") band, referred to as a spin-1 chiral fermion. Three-dimensional spin-1 chiral fermion systems have been theoretically predicted and experimentally observed in chiral crystals [4–11].

Quantum transport phenomena in exhibit nontrivial impurity effects [12–19]. The electrical conductivity behavior near the Dirac point is particularly sensitive to disorder, making a theoretical framework that accurately captures scattering effects essential. The self-consistent Born approximation (SCBA) is a well-established method for this purpose, as it can properly incorporate the disorder-induced broadening of the density of states. Of particular interest is the cusp-like structure in the energy dependence of the electrical conductivity, which originates from the multifold nature of the band crossings and is well described theoretically by employing the SCBA [19–23]. For spin-1 chiral fermions, this cusp structure appears asymmetrically with respect to energy [19]. Such asymmetric cusps in the conductivity are highly intriguing, as they may lead to unconventional thermoelectric responses, which are both theoretically and practically significant.

In this work, we provide a detailed analysis of the conditions under which these cusps emerge and their physical implications. Specifically, we analyze the electrical conductivity of spin-1 chiral fermion systems with disordered potentials using the self-consistent Born approximation (SCBA) combined with vertex corrections. We show that the energy at which the cusp structure emerges, ϵ_c , is determined by the strength of impurity scattering. We find that as the scattering becomes stronger, both $|\epsilon_c|$ and the corresponding conductivity σ_c increase. Our analysis also reveals that a small curvature of the trivial band makes the system more susceptible to scattering, which further enhances the values of $|\epsilon_c|$ and σ_c . These results provide fundamental insights into the transport anomalies originating from multifold band crossings.

2 Model for a Spin-1 Chiral Fermion

We study a three-dimensional spin-1 chiral fermion with rotational and time-reversal symmetries. The system is described by the following effective Hamiltonian [24]:

$$\hat{\mathcal{H}} = \hbar v \, \hat{\mathbf{S}} \cdot \mathbf{k} + c' \left[(\hat{\mathbf{S}} \cdot \mathbf{k})^2 - k^2 \hat{S}_0 \right], \tag{1}$$

where k denotes the wave vector, and v is the Fermi velocity. $\hat{S} = (\hat{S}_x, \hat{S}_y, \hat{S}_z)$ are given in matrix form as follows:

$$\hat{S}_x = \begin{pmatrix} 0 & i & 0 \\ -i & 0 & 0 \\ 0 & 0 & 0 \end{pmatrix}, \quad \hat{S}_y = \begin{pmatrix} 0 & 0 & -i \\ 0 & 0 & 0 \\ i & 0 & 0 \end{pmatrix}, \quad \hat{S}_z = \begin{pmatrix} 0 & 0 & 0 \\ 0 & 0 & i \\ 0 & -i & 0 \end{pmatrix}, \tag{2}$$

and \hat{S}_0 denotes the identity matrix. The second term in Eq. 1, characterized by the parameter c', introduces a quadratic correction to the dispersion. Specifically, this term adds curvature exclusively to the trivial band, leaving the Dirac bands linear. The parameter c' determines the strength of this curvature.

The energy spectrum consists of three bands, with eigenvalues given by

$$\epsilon_{\mathbf{c},\mathbf{k}} = \hbar v k,$$
 (3)

$$\epsilon_{\mathbf{t},\mathbf{k}} = -c'k^2,\tag{4}$$

$$\epsilon_{\mathbf{v},\mathbf{k}} = -\hbar v k,\tag{5}$$

where the subscripts c, t, v correspond to the conduction, trivial, and valence bands, respectively. To investigate the effects of the curvature of the trivial band, we set b'=1 as the simplest model. We also define the dimensionless parameter characterizing the curvature of the trivial band:

$$c = \frac{c'q_0}{\hbar v},\tag{6}$$

where q_0 is the inverse of the characteristic length scale.

To incorporate disorder effects, we consider impurity scattering described by finiterange Gaussian potentials. The real-space form of the impurity potential is given by

$$U(\mathbf{r}) = \frac{\pm u_0}{(\sqrt{\pi}d_0)^3} \exp\left(-\frac{r^2}{d_0^2}\right),\tag{7}$$

where d_0 characterizes the range of the potential, and $\pm u_0$ represents its strength. The sign \pm indicates that the system contains an equal number of positive and negative impurities, ensuring that the Fermi level remains unaffected by the impurity concentration.

The Fourier transform of the potential is computed as

$$u(\mathbf{k}) = \int d^3 r \, e^{-i\mathbf{k}\cdot\mathbf{r}} U(\mathbf{r}) = \pm u_0 \exp\left(-\frac{k^2}{q_0^2}\right),\tag{8}$$

where the inverse length scale is defined as $q_0 = 2/d_0$. The scattering strength is quantified by the parameter W, given by

$$W = \frac{q_0 n_i u_0^2}{\hbar^2 v^2}. (9)$$

Here, n_i denotes the number of scatterers per unit volume.

3 Self-Consistent Born Approximation

Assuming that impurities are randomly and uniformly distributed, the disorder-averaged Green's function takes the form

$$\hat{G}(\mathbf{k}, \epsilon + is0) = \left[\epsilon \hat{S}_0 - \hat{\mathcal{H}} - \hat{\Sigma}(\mathbf{k}, \epsilon + is0)\right]^{-1},\tag{10}$$

The index $s=\pm 1$ distinguishes between the retarded (s=1) and advanced (s=-1) Green's functions.

The self-energy $\hat{\Sigma}$ is determined self-consistently via the integral equation

$$\hat{\Sigma}(\mathbf{k}, \epsilon + is0) = \int \frac{d\mathbf{k}'}{(2\pi)^3} n_i |u(\mathbf{k} - \mathbf{k}')|^2 \hat{G}(\mathbf{k}', \epsilon + is0). \tag{11}$$

The conductivity $\sigma(\epsilon)$ at zero temperature, calculated using the Kubo formalism, is given by

$$\sigma(\epsilon) = -\frac{\hbar e^2 v^2}{4\pi} \sum_{s,s'=\pm 1} ss' \int \frac{d\mathbf{k}' d\epsilon}{(2\pi)^3} \times \text{Tr} \left[\frac{\hat{v}_x}{v} \, \hat{G}(\mathbf{k}', \epsilon + is0) \, \hat{J}_x(\mathbf{k}', \epsilon + is0, \epsilon + is'0) \, \hat{G}(\mathbf{k}', \epsilon + is'0) \right], \tag{12}$$

where the velocity operator in the x-direction is defined as

$$\hat{v}_x = \frac{1}{\hbar} \frac{\partial \hat{\mathcal{H}}}{\partial k_x}.$$
 (13)

The current vertex function \hat{J}_x , incorporating vertex corrections, satisfies the Bethe–Salpeter equation:

$$\hat{J}_x(\mathbf{k}, \epsilon, \epsilon') = \frac{\hat{v}_x}{v} + \int \frac{d\mathbf{k'}}{(2\pi)^3} n_i |u(\mathbf{k} - \mathbf{k'})|^2 \hat{G}(\mathbf{k'}, \epsilon) \hat{J}_x(\mathbf{k'}, \epsilon, \epsilon') \hat{G}(\mathbf{k'}, \epsilon'). \tag{14}$$

To clarify the physical origins of various contributions in a multiband system, we diagonalize the Green's function in the band basis:

$$\hat{U}^{\dagger}\hat{G}(\mathbf{k}, \epsilon + is0)\hat{U} = \begin{pmatrix} G_{c}^{s} & 0 & 0\\ 0 & G_{0}^{s} & 0\\ 0 & 0 & G_{v}^{s} \end{pmatrix},$$
(15)

where the labels c, 0, and v correspond to the conduction, trivial, and valence bands, respectively. In this basis, the velocity and vertex operators are represented as:

$$\frac{1}{v}\hat{U}^{\dagger}\hat{v}_{x}\hat{U} = \begin{pmatrix} v_{\text{cc}} & v_{\text{c0}} & 0\\ v_{0\text{c}} & v_{00} & v_{0\text{v}}\\ 0 & v_{\text{vo}} & v_{\text{vv}} \end{pmatrix}, \quad \hat{U}^{\dagger}\hat{J}_{x}(\boldsymbol{k}, \epsilon + is0, \epsilon + is'0)\hat{U} = \begin{pmatrix} J_{\text{cc}}^{ss'} & J_{\text{co}}^{ss'} & J_{\text{ss}}^{ss'}\\ J_{\text{cc}}^{ss'} & J_{\text{co}}^{ss'} & J_{\text{co}}^{ss'}\\ 0 & J_{\text{vo}}^{ss'} & J_{\text{vv}}^{ss'} \end{pmatrix}. \quad (16)$$

The total conductivity is decomposed into physically distinct contributions as follows. The intraband part within the Dirac bands (conduction and valence) is given by:

$$-\frac{\hbar e^2 v^2}{4\pi} \sum_{s,s'=\pm 1} ss' \int d\epsilon \int \frac{d\mathbf{k'}}{(2\pi)^3} \left(v_{\rm cc} G_{\rm c}^s J_{\rm cc}^{ss'} G_{\rm c}^{s'} + v_{\rm vv} G_{\rm v}^s J_{\rm vv}^{ss'} G_{\rm v}^{s'} \right). \tag{17}$$

The interband term involving the Dirac and trivial bands reads:

$$-\frac{\hbar e^2 v^2}{4\pi} \sum_{s,s'=\pm 1} ss' \int d\epsilon \int \frac{d\mathbf{k'}}{(2\pi)^3} \times \left(v_{0c} G_c^s J_{c0}^{ss'} G_0^{s'} + v_{c0} G_0^s J_{0c}^{ss'} G_c^{s'} + v_{0v} G_v^s J_{v0}^{ss'} G_0^{s'} + v_{v0} G_0^s J_{0v}^{ss'} G_v^{s'} \right).$$
(18)

Finally, the intraband contribution within the trivial band is:

$$-\frac{\hbar e^2 v^2}{4\pi} \sum_{s,s'=\pm 1} ss' \int d\epsilon \int \frac{d\mathbf{k}'}{(2\pi)^3} v_{00} G_0^s J_{00}^{ss'} G_0^{s'}.$$
 (19)

Details of the derivation and numerical calculations are given in Ref. [19].

4 Cusped Electrical Conductivity

Figure 1 illustrates the energy dependence of the electrical conductivity in a spin-1 chiral fermion system at absolute zero temperature. A distinct cusp structure is observed in the conductivity spectrum. We define the energy at which the cusp appears as the characteristic energy ϵ_c . Importantly, this cusp does not occur precisely at the band crossing point $\epsilon=0$, but rather slightly deviates from it. The absolute value $|\epsilon_c|$ increases with increasing impurity strength W and decreasing curvature parameter |c|. This behavior can be understood in terms of a band-resolved analysis, as explained below.

As shown in Fig. 2(d), the intraband contribution from the trivial band drops rapidly below ϵ_c , while that from the Dirac bands rises sharply above ϵ_c , forming the cusp. In this context, the cusp structure arises as a distinctive feature stemming from the multiband-crossing nature of the system. Figures 2(d)–(f) reveal that, due to impurity scattering, the energy of the cusp ϵ_c is slightly shifted from the Dirac point. As W increases, not only does $|\epsilon_c|$ grow due to enhanced scattering, but the conductivity

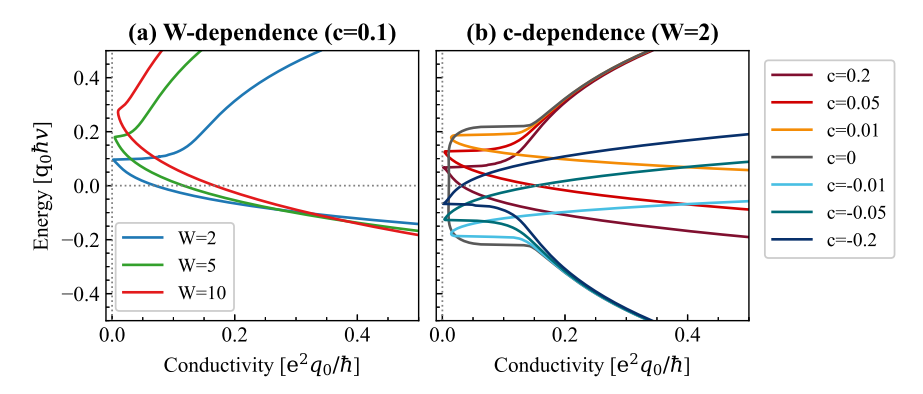


Fig. 1: (Color online) Conductivity as a function of energy for various values of the impurity parameter W and the curvature parameter c. Panel (a) shows the W-dependence of the conductivity spectra at a fixed curvature c = 0.1, for W = 2, 5, 10. Panel (b) shows the c-dependence at a fixed impurity strength W = 2, for c = -0.2 to 0.2.

contributions — both intraband and interband — also become smoother as functions of energy. This results in a more gradual cusp shape.

The value of ϵ_c is determined not only by the impurity parameter W but also by the curvature parameter c. Figure 3 presents the energy dependence of the conductivity for various values of c, with the impurity strength fixed, emphasizing the distinct contributions from different scattering channels. In the special case of c=0, the intraband contribution from the trivial band becomes exactly zero, and no cusp appears in the conductivity spectrum. For $c \neq 0$, however, the intraband contribution from the trivial band becomes finite and plays a key role in the emergence of the cusp structure. As |c| decreases, $|\epsilon_c|$ increases. This trend can be attributed to the enhancement of the density of states near the Dirac point at smaller |c|, rendering the system more susceptible to impurity scattering. Consequently, smaller |c| results in a smoother energy dependence of the conductivity, leading to a more gradual cusp shape.

In summary, these results demonstrate that the cusp structure is a prominent manifestation of the multifold band structure inherent to spin-1 chiral fermion systems. Physically, this cusp is formed by the competition between two transport channels with opposite energy dependencies: the intraband conduction within the Dirac bands and that within the trivial band of finite curvature. Impurity scattering plays a decisive role by broadening the energy levels near the Dirac point, which mixes the contributions from both channels. Consequently, the scattering strength W and the trivial band curvature c sensitively control the cusp's position ϵ_c and its corresponding conductivity σ_c . This physical picture, where impurity-induced level broadening is key to the formation of the cusp, underscores that the SCBA, which self-consistently incorporates this effect, is an essential framework for theoretically describing this phenomenon.

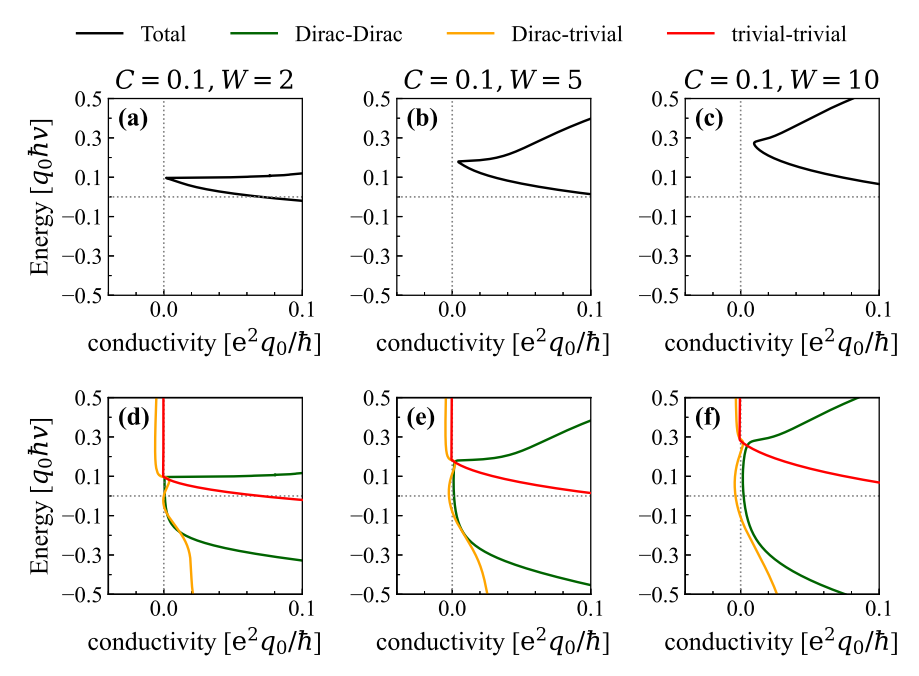


Fig. 2: (Color online) Conductivity as a function of energy for different impurity strengths W=2,5,10 with fixed curvature parameter c=0.1. The upper panels (a–c) show the total conductivity, while the lower panels (d-f) show the decomposed contributions: green lines correspond to intraband processes within Dirac bands ("Dirac–Dirac"), orange lines to interband processes between Dirac and trivial bands ("Dirac–trivial"), and red lines to intraband processes within trivial bands ("trivial–trivial").

5 Conclusion

In this study, we have analyzed the electrical conductivity of spin-1 chiral fermion systems with disordered potentials using the self-consistent Born approximation (SCBA) combined with vertex corrections. We found that the cusp structure appears in the energy dependence of the conductivity and originates from the multiband nature, as examined through the band decomposition of the conductivity. Our results highlight that capturing the impurity-induced energy broadening near the Dirac point is essential for describing the cusp structure, making the SCBA an effective framework for this analysis. The energy ϵ_c at which the cusp emerges is determined by the strength of impurity scattering. As the scattering becomes stronger, both $|\epsilon_c|$ and the corresponding conductivity σ_c increase. Moreover, when the curvature of the trivial band is small, the system becomes more susceptible to scattering, leading to further increases in $|\epsilon_c|$ and σ_c . This unconventional energy dependence of the conductivity arises from the crossing of multiple energy bands protected by crystal symmetry. These findings

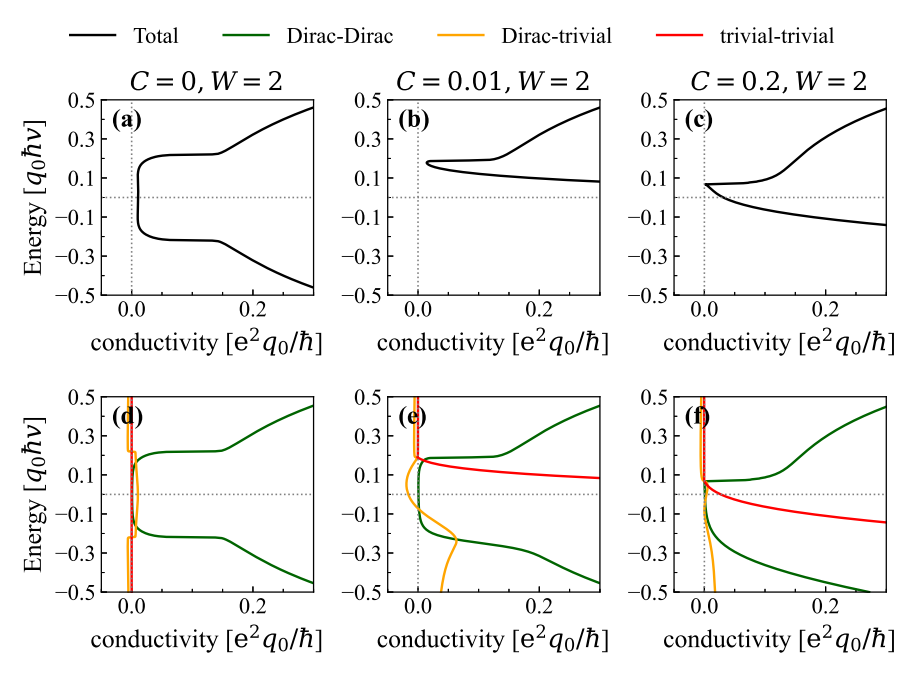


Fig. 3: (Color online) Conductivity as a function of energy for different curvatures c=0,0.01,0.2 with fixed impurity strength W=2. The upper panels (a-c) show the total conductivity, while the lower panels (d-f) show the decomposed contributions: green lines correspond to intraband processes within Dirac bands ("Dirac–Dirac"), orange lines to interband processes between Dirac and trivial bands ("Dirac–trivial"), and red lines to intraband processes within trivial bands ("trivial–trivial").

serve as a basis for future investigations into novel transport phenomena in topological semimetals.

Acknowledgements. This work was supported by JSPS KAKENHI (Grant Nos. JP25KJ1427, JP25K07224, and JP24H00853).

References

- [1] J.L. Mañes, Existence of bulk chiral fermions and crystal symmetry. Phys. Rev. B 85, 155118 (2012). https://doi.org/10.1103/PhysRevB.85.155118
- [2] B. Bradlyn, J. Cano, Z. Wang, M.G. Vergniory, C. Felser, R.J. Cava, B.A. Bernevig, Beyond Dirac and Weyl fermions: Unconventional quasi-particles in conventional crystals. Science **353**(6299), aaf5037 (2016). https://doi.org/10.1126/science.aaf5037

- [3] B.Q. Lv, T. Qian, H. Ding, Experimental perspective on threedimensional topological semimetals. Rev. Mod. Phys. 93, 025002 (2021). https://doi.org/10.1103/RevModPhys.93.025002
- [4] P. Tang, Q. Zhou, S.C. Zhang, Multiple Types of Topological Fermions in Transition Metal Silicides. Phys. Rev. Lett. 119, 206402 (2017). https://doi.org/10.1103/PhysRevLett.119.206402
- [5] G. Chang, S.Y. Xu, B.J. Wieder, D.S. Sanchez, S.M. Huang, I. Belopolski, T.R. Chang, S. Zhang, A. Bansil, H. Lin, M.Z. Hasan, Unconventional Chiral Fermions and Large Topological Fermi Arcs in RhSi. Phys. Rev. Lett. 119, 206401 (2017). https://doi.org/10.1103/PhysRevLett.119.206401
- [6] D.A. Pshenay-Severin, Y.V. Ivanov, A.A. Burkov, A.T. Burkov, Band structure and unconventional electronic topology of CoSi. J. Phys.: Condens. Matter 30(13), 135501 (2018). https://doi.org/10.1088/1361-648X/aab0ba
- [7] D. Takane, Z. Wang, S. Souma, K. Nakayama, T. Nakamura, H. Oinuma, Y. Nakata, H. Iwasawa, C. Cacho, T. Kim, K. Horiba, H. Kumigashira, T. Takahashi, Y. Ando, T. Sato, Observation of Chiral Fermions with a Large Topological Charge and Associated Fermi-Arc Surface States in CoSi. Phys. Rev. Lett. 122, 076402 (2019). https://doi.org/10.1103/PhysRevLett.122.076402
- [8] Z. Rao, H. Li, T. Zhang, S. Tian, C. Li, B. Fu, C. Tang, L. Wang, Z. Li, W. Fan, J. Li, Y. Huang, Z. Liu, Y. Long, C. Fang, H. Weng, Y. Shi, H. Lei, Y. Sun, T. Qian, H. Ding, Observation of unconventional chiral fermions with long Fermi arcs in CoSi. Nature 567(7749), 496–499 (2019). https://doi.org/10.1038/s41586-019-1031-8
- [9] D.S. Sanchez, I. Belopolski, T.A. Cochran, X. Xu, J.X. Yin, G. Chang, W. Xie, K. Manna, V. Süß, C.Y. Huang, N. Alidoust, D. Multer, S.S. Zhang, N. Shumiya, X. Wang, G.Q. Wang, T.R. Chang, C. Felser, S.Y. Xu, S. Jia, H. Lin, M.Z. Hasan, Topological chiral crystals with helicoid-arc quantum states. Nature 567(7749), 500–505 (2019). https://doi.org/10.1038/s41586-019-1037-2
- [10] S. Mozaffari, N. Aryal, R. Schönemann, K.W. Chen, W. Zheng, G.T. McCandless, J.Y. Chan, E. Manousakis, L. Balicas, Multiple Dirac nodes and symmetry protected Dirac nodal line in orthorhombic α -RhSi. Phys. Rev. B **102**, 115131 (2020). https://doi.org/10.1103/PhysRevB.102.115131
- [11] I. Robredo, N.B.M. Schröter, C. Felser, J. Cano, B. Bradlyn, M.G. Vergniory, Multifold topological semimetals. Europhysics Letters **147**(4), 46001 (2024). https://doi.org/10.1209/0295-5075/ad6bbc
- [12] E.R. Mucciolo, C.H. Lewenkopf, Disorder and electronic transport in graphene. Journal of Physics: Condensed Matter **22**(27), 273201 (2010). https://doi.org/10.1088/0953-8984/22/27/273201. URL

- [13] M. Vigh, L. Oroszlány, S. Vajna, P. San-Jose, G. Dávid, J. Cserti, B. Dóra, Diverging dc conductivity due to a flat band in a disordered system of pseudospin-1 Dirac-Weyl fermions. Phys. Rev. B 88, 161413(R) (2013). https://doi.org/10.1103/PhysRevB.88.161413
- [14] S.V. Syzranov, L. Radzihovsky, High-dimensional disorder-driven phenomena in Weyl semimetals, semiconductors, and related systems. Annual Review of Condensed Matter Physics 9(1), 35–58 (2018). https://doi.org/10.1146/annurev-conmatphys-033117-054037. URL https://doi.org/10.1146/annurev-conmatphys-033117-054037
- [15] R. Kikuchi, T. Funato, A. Yamakage, Quantum transport of a spin-1 chiral fermion. Phys. Rev. B **106**, 235204 (2022). https://doi.org/10.1103/PhysRevB.106.235204
- [16] H.C. Hsu, I.C. Fulga, J.S. You, Disorder effects on triple-point fermions. Phys. Rev. B 106, 245118 (2022). https://doi.org/10.1103/PhysRevB.106.245118
- [17] R. Kikuchi, A. Yamakage, Electrical conductivity and screening effect of spin-1 chiral fermions scattered by charged impurities. Phys. Rev. B 108, 085204 (2023). https://doi.org/10.1103/PhysRevB.108.085204
- [18] V. Leeb, J. Knolle, Theory of difference-frequency quantum oscillations. Phys. Rev. B 108, 054202 (2023). https://doi.org/10.1103/PhysRevB.108.054202
- [19] R. Kikuchi, A. Yamakage, Band curvature effects on quantum transport of spin-1 chiral fermion systems. Phys. Rev. B 111, 125201 (2025). https://doi.org/10.1103/PhysRevB.111.125201
- [20] N.H. Shon, T. Ando, Quantum Transport in Two-Dimensional Graphite System. J. Phys. Soc. Jpn. $\mathbf{67}(7)$, 2421-2429 (1998). https://doi.org/10.1143/JPSJ.67.2421
- [21] M. Noro, M. Koshino, T. Ando, Theory of Transport in Graphene with Long-Range Scatterers. J. Phys. Soc. Jpn. 79(9), 094713 (2010). https://doi.org/10.1143/JPSJ.79.094713
- [22] Y. Ominato, M. Koshino, Quantum transport in a three-dimensional Weyl electron system. Phys. Rev. B 89, 054202 (2014). https://doi.org/10.1103/PhysRevB.89.054202
- [23] Y. Ominato, M. Koshino, Quantum transport in three-dimensional Weyl electron system in the presence of charged impurity scattering. Phys. Rev. B **91**, 035202 (2015). https://doi.org/10.1103/PhysRevB.91.035202

[24] S. Mandal, J.M. Link, I.F. Herbut, Time-reversal symmetry breaking and d-wave superconductivity of triple-point fermions. Phys. Rev. B $\bf 104$, 134512 (2021). https://doi.org/10.1103/PhysRevB.104.134512